

Decrease in electrical contact resistance of Sb-doped n+-BaSi₂ layers and spectral response of an Sb-doped n+-BaSi₂/undoped BaSi₂ structure for solar cells

著者別名	都甲 薫, 未益 崇
journal or publication title	Japanese journal of applied physics
volume	57
number	3
page range	031202
year	2018-02
権利	(C) 2017 The Japan Society of Applied Physics
URL	http://hdl.handle.net/2241/00150696

doi: 10.7567/JJAP.57.031202

Decrease in electrical contact resistance of Sb-doped n⁺-BaSi₂ layers and spectral response of an Sb-doped n⁺-BaSi₂/undoped BaSi₂ structure for solar cells

Komomo Kodama, Ryota Takabe, Suguru Yachi, Kaoru Toko, Takashi Suemasu*

Institute of Applied Physics, Graduate School of Pure and Applied Sciences, University of Tsukuba, Tsukuba, Ibaraki 305-8573, Japan

We investigated how the electron concentration n in a 300-nm-thick Sb-doped n⁺-BaSi₂ layer grown by molecular beam epitaxy affected the contact resistance R_C to surface electrodes (Al, indium-tin-oxide). As the n of n-BaSi₂ increased, R_C decreased and reached a minimum of 0.019 Ω cm² at $n = 2.4 \times 10^{18}$ cm⁻³ for the Al electrodes. This value was more than one order of magnitude smaller than that obtained for Al/B-doped p-BaSi₂. We believe that this significant decrease in R_C came from Sb segregation. Furthermore, the internal quantum efficiency (*IQE*) spectrum was evaluated for an Sb-doped n⁺-BaSi₂(20 nm)/undoped BaSi₂(500 nm)/n⁺-Si(111) structure. Its *IQE* reached as high as ~50% over a wide wavelength range under a small bias voltage of 0.1 V applied between the top and bottom electrodes.

Email: suemasu@bk.tsukuba.ac.jp

1. Introduction

In many studies, various solar cells materials such as CdTe, chalcopyrites, kesterite, and perovskite have been assessed because of their low cost and high efficiency [1-6]. However, these materials contain elements that are scarce, toxic, or both. Thin-film Si solar cells have also been studied extensively; however, it is not easy to achieve efficiencies as high as 20% [7-17]. Thus, it is important to explore other materials for thin-film solar cells. Among such materials, we have focused on barium disilicide (BaSi_2), a semiconductor consisting of only abundant elements [18,19]. BaSi_2 is attractive for use in thin-film solar cells because of its bandgap of 1.3 eV, a matching solar spectrum [20], a high absorption coefficient of $3 \times 10^4 \text{ cm}^{-1}$ at 1.5 eV comparable to those of chalcopyrites [21-23], and superior minority-carrier diffusion length ($L \sim 10 \text{ }\mu\text{m}$) [24,25] and lifetime ($\tau \sim 10 \text{ }\mu\text{s}$) [26-29]. Because of these properties, an energy conversion efficiency η of over 25% can be expected for a 2- μm -thick BaSi_2 pn-junction diode [30]. Recently, we have achieved a conversion efficiency near 10% with B-doped p- BaSi_2 /n-Si heterojunction solar cells [31].

To fabricate BaSi_2 homojunction solar cells, we plan to use undoped BaSi_2 as an absorber layer in a solar cell. Undoped BaSi_2 has both a high α and a large L , both of which facilitate the collection of photogenerated carriers in an external circuit even though L degrades somewhat because of extrinsic effects such as crystal imperfections. In a solar cell, the topmost layer should be a heavily impurity-doped n- or p-type layer to decrease the contact resistance R_C , which directly affects the fill factor FF of the solar cell. As R_C increases, FF decreases and thus η decreases. In many studies, R_C have been assessed in solar cell materials [32-38]. In our previous work, we investigated the R_C between Al electrodes and B-doped p- BaSi_2 . The R_C reached a minimum of $0.35 \text{ }\Omega \text{ cm}^2$ [31] when the hole concentration p of p- BaSi_2 was $4.0 \times 10^{18} \text{ cm}^{-3}$. In this study, we first investigated the dependence of R_C between surface electrodes (Al or ITO) and Sb-doped n- BaSi_2 layers at various electron concentrations. We then evaluated the

spectral response of an Sb-doped n^+ -BaSi₂(20 nm)/undoped BaSi₂(500 nm) structure to verify how the heavily doped n^+ -BaSi₂ surface layer affected the spectral response, especially at short wavelengths.

2. Experimental methods

Here, we used an ion-pumped molecular beam epitaxy (MBE) system equipped with an electron-beam evaporation source for Si as well as standard Knudsen cells for Ba and Sb. Details of the growth procedure of undoped BaSi₂ and Sb-doped n -BaSi₂ were reported previously [39,40]. To measure R_C , we used high-resistivity Czochralski (CZ) p-Si(111) substrates (resistivity $\rho = 1000\text{--}10000 \text{ } \Omega \text{ cm}$) to minimize current flowing through the substrate. After thermally cleaning the substrate at the substrate temperature $T_S = 900 \text{ } ^\circ\text{C}$, we deposited Ba at $500 \text{ } ^\circ\text{C}$ to form an approximately 5-nm-thick BaSi₂ template layer by reactive deposition epitaxy. This template worked as seeds that control the crystal orientation of the BaSi₂ overlayers [41]. Next, we formed 300-nm-thick Sb-doped n -BaSi₂ epitaxial layers by MBE at various T_S values of 460 (sample A), 480 (sample B), 500 (sample C), and $520 \text{ } ^\circ\text{C}$ (sample D). The electron concentration n of Sb-doped n -BaSi₂ depends on T_S [40]. Then, a 3-nm-thick a-Si passivation layer was deposited *in situ* at $T_S = 180 \text{ } ^\circ\text{C}$ [42]. Finally, 150-nm-thick striped Al or ITO electrodes (length $l = 0.6 \text{ mm}$, width $W = 7.0 \text{ mm}$, electrode interval $d = 1.0 \text{ mm}$) were formed by sputtering. Carrier concentration was measured by the van der Pauw method at room temperature (RT). R_C was measured by the transfer length method at RT [43]. We compared the smallest R_C , $R_C = 0.35 \text{ } \Omega \text{ cm}^2$, measured from Al/p-BaSi₂ ($p = 4.0 \times 10^{18} \text{ cm}^{-3}$, sample E) [31]. The depth profile of Sb atoms was measured by secondary ion mass spectrometry (SIMS) using Cs^+ ions.

Next, we investigated the photoresponse properties of the Sb-doped n^+ -BaSi₂/undoped BaSi₂ structure (sample F). A 500-nm-thick undoped BaSi₂ layer was epitaxially grown on a

low-resistivity Cz n-Si(111) substrate ($\rho < 0.01 \text{ } \Omega \text{ cm}$) at $T_S = 580 \text{ } ^\circ\text{C}$, followed by a 20-nm-thick Sb-doped n⁺-BaSi₂ ($n = 2.4 \times 10^{18} \text{ cm}^{-3}$) layer and a 3-nm-thick a-Si passivation layer. We used the low-resistivity Si substrate to exclude the contribution of photogenerated carriers in the n-Si substrate and to form a good electrical contact at the BaSi₂/Si heterointerface. Finally, 80-nm-thick ITO electrodes with a diameter of 1 mm and 150-nm-thick Al rear electrodes were formed by sputtering. The reflectance R and external quantum efficiency (EQE) spectra were evaluated at RT using a lock-in technique with a xenon lamp and a single monochromator (Bunko Keiki, SM-1700A and RU-60N) with a focal length of 25 cm. Internal quantum efficiency (IQE) was obtained by dividing the EQE by $(1-R)$. Light intensity was calibrated using a pyroelectric sensor (Melles Griot, 13PEM001/J). The crystalline quality of the grown layers was characterized by reflection high-energy electron diffraction (RHEED) and X-ray diffraction (XRD) analyses using Cu K α radiation.

3. Results and discussion

Figure 1 shows the θ - 2θ XRD and RHEED patterns of samples A, B, C, and D. The RHEED patterns were observed along the Si $[1\bar{1}2]$ azimuth. The diffraction peaks appeared only from the (100)-oriented BaSi₂ planes, such as (200), (400), and (600), showing that a -axis-oriented BaSi₂ epitaxial films were formed. However, the RHEED patterns were not streaky but spotty, meaning that the surface is rough. This surface roughness developed because the T_S for Sb-doped BaSi₂ was much lower [40] than the optimum T_S ($\sim 600 \text{ } ^\circ\text{C}$) for the undoped BaSi₂ absorber layers. The n values of samples A, B, C, and D were 6.9×10^{17} , 1.8×10^{18} , 2.4×10^{18} , and $2.8 \times 10^{17} \text{ cm}^{-3}$, respectively. Now, using sample C as an example, we will show how to obtain R_C . Figure 2 shows the relationship between the measured resistance $r(x)$ between the Al or ITO electrodes and the electrode distance x for sample C ($n = 2.4 \times 10^{18} \text{ cm}^{-3}$, $\mu = 100 \text{ cm}^2/\text{V s}$). Ignoring the lateral resistance of the electrode when the current flows in the x direction,

$r(x)$ can be written as

$$r(x) \approx 2r_c + r_{\text{semi}}(x), \quad (1)$$

where $r_{\text{semi}}(x)$ is the resistance of the semiconductor and $2r_c$ is the intercept of the vertical axis when we plot $r(x)$ with respect to x . Because the second term on the right side of Eq. (1) is proportional to x , $r(x)$ increases with increasing x . As shown in Fig. 2, the line for the ITO electrodes has a slightly higher slope and thus a larger resistance than that for Al electrodes. This behavior probably occurred because the ITO electrode had larger lateral resistance than Al. From the plots in Fig. 2, $r_c = 2.26$ and $1.22 \text{ } \Omega$ were obtained for the ITO and Al electrodes, respectively. R_C is given by

$$R_C = r_c \times W \times L_t, \quad (2)$$

where L_t is the transfer length, which is half of the intercept of the horizontal axis of the straight line in Fig. 2. From Eq. (2), R_C was calculated to be 0.057 and $0.019 \text{ } \Omega \text{ cm}^2$ for the ITO and Al electrodes, respectively, in sample C.

Figure 3 summarizes the dependence of R_C on n for all the samples obtained by the method described above. R_C decreased with increasing n . The smallest R_C , $0.019 \text{ } \Omega \cdot \text{cm}^2$, was obtained from Al electrodes in sample C. This value is more than one order of magnitude smaller than the smallest R_C ($0.35 \text{ } \Omega \text{ cm}^2$) obtained from Al/B-doped p-BaSi₂ ($p = 4.0 \times 10^{18} \text{ cm}^{-3}$, $\mu = 28 \text{ cm}^2 \text{V}^{-1} \text{ s}^{-1}$) [31]. We will now discuss the reason for this behavior. According to Ref. 36, the sheet resistance R_{sheet} is given by

$$R_{\text{sheet}} = R_C / L_t^2. \quad (2)$$

For sample C, R_{sheet} is $0.40 \text{ } \Omega$ from $L_t = 0.218 \text{ mm}$ and $R_C = 0.019 \text{ } \Omega \text{ cm}^2$, while R_{sheet} equals $6.79 \text{ } \Omega$ using $L_t = 0.227 \text{ mm}$ and $R_C = 0.35 \text{ } \Omega \cdot \text{cm}^2$ for sample E. Such a large difference in R_{sheet} between samples C and E cannot be anticipated from their similar ρ values: 0.0644 and $0.0557 \text{ } \Omega \text{ cm}$, respectively, which were determined by Hall measurements. It is known that B atoms in B-doped p-BaSi₂ do not segregate and so are almost uniformly distributed [44]. Figure 4 shows

the depth profile of Sb atoms and secondary ions (Ba + Si) in sample C. The Sb atoms segregate toward the surface of sample C, and the Sb concentration exceeds 10^{20} cm^{-3} near the electrode. Segregation of Sb has been observed in various semiconductors such as Si, Ge, and III–V semiconductors [45-52]. Hence, n is actually much higher in the surface region than the n found from the Hall measurement ($n = 2.4 \times 10^{18} \text{ cm}^{-3}$), leading to the significant decrease in R_{sheet} and thus R_c in sample C. Owing to the segregation of Sb in BaSi₂, an Sb-doped n⁺-BaSi₂ layer should be placed on the top of the BaSi₂ solar cell. Hence, an Sb-doped n⁺-BaSi₂/undoped BaSi₂ absorber layered structure is useful for practical applications.

We next assessed the spectral response of sample F, with an Sb-doped n⁺-BaSi₂/undoped BaSi₂ structure. Figure 5 shows a schematic of sample F for this purpose and the RHEED patterns obtained after the growth of each layer. Because BaSi₂ has a large α , short-wavelength light is absorbed near the surface, in the Sb-doped n⁺-BaSi₂ layer. Therefore, defective n⁺-BaSi₂ deteriorates the solar-cell performance. Figure 6 shows the θ - 2θ XRD pattern, revealing a -axis-oriented epitaxial growth up to the 20-nm-thick Sb-doped n⁺-BaSi₂. Figure 7 shows the *IQE* spectrum of sample F. A bias voltage of -0.1 V was applied to the top ITO electrode with respect to the back side-surface Al electrode so that the photogenerated holes in the BaSi₂ were extracted into the ITO electrode. The *IQE* increased sharply at wavelengths shorter than approximately 1000 nm, corresponding to the band gap of BaSi₂, and reached approximately 50% over a wide wavelength range even under this small bias voltage. We observed no pronounced reduction in *IQE* at short wavelengths, even when a highly Sb-doped layer was inserted. In a BaSi₂ homojunction solar cell, the built-in potential across the pn junction will be much higher than 0.1 V, producing larger *IQEs*. On the basis of these findings, we conclude that the Sb-doped n⁺-BaSi₂/undoped BaSi₂ absorber layered structure is suitable for practical BaSi₂ solar cells.

4. Conclusions

We investigated the dependence of R_C on the electron concentration of Sb-doped n-BaSi₂ and achieved a minimum R_C of 0.019 $\Omega \text{ cm}^2$ for Al/Sb-doped n-BaSi₂ at $n = 2.4 \times 10^{18} \text{ cm}^{-3}$. This R_C was more than one order of magnitude smaller than the R_C obtained for Al/B-doped p-BaSi₂, 0.35 $\Omega \cdot \text{cm}^2$. We explained this significant reduction in R_C in Al/Sb-doped n-BaSi₂ as being due to Sb segregation, which was verified by SIMS. The concentration of Sb atoms exceeded 10^{20} cm^{-3} near the electrode, significantly decreasing R_C . We achieved an $IQE > 50\%$ over a wide wavelength range under a small bias voltage of 0.1 V in the n⁺(20 nm)/undoped BaSi₂(500 nm)/n⁺-Si(111) structure.

Acknowledgements

This work was financially supported by JSPS KAKENHI Grant Numbers 15H02237 and 17K18865. R.T. was financially supported by a Grant-in-Aid for JSPS Fellows (15J02139).

References

- [1] M. G. Panthani, V. Akhavan, B. Goodfellow, J. P. Schmidtke, L. Dunn, A. Dodabalapur, P. F. Barbara, and B. A. Korgel, *J. Am. Chem. Soc.* **130**, 16770 (2008).
- [2] W. Jaegermann, A. Klein, and T. Mayer, *Adv. Mater.* **21**, 4196 (2009).
- [3] S. Ahmed, K. B. Reuter, O. Gunawan, L. Guo, L. T. Romankiw, and H. Deligianni, *Adv. Energy Mater.* **2**, 253 (2012).
- [4] C. Steinhagen, M. G. Panthani, V. Akhavan, B. Goodfellow, B. Koo, and B. A. Korgel, *J. Am. Chem. Soc.* **131**, 12554 (2009).
- [5] M. A. Green, A. Ho-Baillie, and H. J. Snaith, *Nat. Photonics* **8**, 506 (2014).
- [6] H. S. Kim, S. H. Im, and N. G. Park, *J. Phys. Chem. C* **118**, 5615 (2014).
- [7] R. G. Gordon, J. Proscia, F. B. Ellis, Jr., and A. E. Delahoy, *Sol. Energy Mater.* **18**, 263 (1989).
- [8] P. Campbell, *Sol. Energy Mater.* **21**, 165 (1990).
- [9] H. Sasaki, H. Morikawa, Y. Matsuno, M. Deguchi, T. Ishihara, H. Kumabe, T. Murotani, and S. Mitsui, *Jpn. J. Appl. Phys.* **33**, 3389 (1994).
- [10] J. Meier, S. Dubail, R. Platz, P. Torres, U. Kroll, J. A. A. Selvan, N. P. Vaucher, Ch. Hof, D. Fischer, H. Keppner, R. Flückiger, A. Shah, V. Shklover, and K.-D. Ufert, *Sol. Energy Mater. Sol. Cells* **49**, 35 (1997).
- [11] O. Vetterl, F. Finger, R. Carius, P. Hapke, L. Houben, O. Kluth, A. Lambertz, A. Mück, B. Rech, and H. Wagner, *Sol. Energy Mater. Sol. Cells* **62**, 97 (2000).
- [12] A. Poruba, A. Fejfar, Z. Remes, J. Springer, M. Vanecek, and J. Kocka, *J. Appl. Phys.* **88**, 148 (2000).
- [13] J. Müller, B. Rech, J. Springer, and M. Vanecek, *Sol. Energy* **77**, 917 (2004).
- [14] M. Berginski, J. Hüpkes, M. Schulte, G. Schöpe, H. Stiebig, and B. Rech, *J. Appl. Phys.* **101**, 074903 (2007).

- [15] D. Zhou and R. Biswas, *J. Appl. Phys.* **103**, 093102 (2008).
- [16] A. Hongsingthong, T. Krajangsang, I. A. Yunaz, S. Miyajima, and M. Konagai, *Appl. Phys. Express* **3**, 051102 (2010).
- [17] H. Sai, Y. Kanamori, and M. Kondo, *Appl. Phys. Lett.* **98**, 113502 (2011).
- [18] J. Evers, G. Oehlinger, and A. Weiss, *Angew. Chem., Int. Ed.* **16**, 659 (1977).
- [19] M. Imai and T. Hirano, *J. Alloys Compd.* **224**, 111 (1995).
- [20] K. Morita, Y. Inomata, and T. Suemasu, *Thin Solid Films* **508**, 363 (2006).
- [21] D. B. Migas, V. L. Shaposhnikov, and V. E. Borisenko, *Phys. Status Solidi B* **244**, 2611 (2007).
- [22] K. Toh, T. Saito, and T. Suemasu, *Jpn. J. Appl. Phys.* **50**, 068001 (2011).
- [23] M. Kumar, N. Umezawa, and M. Imai, *J. Appl. Phys.* **115**, 203718 (2014).
- [24] M. Baba, K. Toh, K. Toko, N. Saito, N. Yoshizawa, K. Jiptner, T. Sakiguchi, K. O. Hara, N. Usami, and T. Suemasu, *J. Cryst. Growth* **348**, 75 (2012).
- [25] M. Baba, K. Watanabe, K. O. Hara, K. Toko, T. Sekiguchi, N. Usami, and T. Suemasu, *Jpn. J. Appl. Phys.* **53**, 078004 (2014).
- [26] K. O. Hara, N. Usami, K. Toh, M. Baba, T. Toko, and T. Suemasu, *J. Appl. Phys.* **112**, 083108 (2012).
- [27] K. O. Hara, N. Usami, K. Nakamura, R. Takabe, M. Baba, K. Toko, and T. Suemasu, *Appl. Phys. Express* **6**, 112302 (2013).
- [28] R. Takabe, K. O. Hara, M. Baba, W. Du, N. Shimada, K. Toko, N. Usami, and T. Suemasu, *J. Appl. Phys.* **115**, 193510 (2014).
- [29] T. Suemasu and N. Usami, *J. Phys. D Appl. Phys.* **50**, 023001 (2017).
- [30] T. Suemasu, *Jpn. J. Appl. Phys.* **54**, 07JA01 (2015).
- [31] S. Yachi, R. Takabe, K. Toko, and T. Suemasu, *Appl. Phys. Lett.* **109**, 072103 (2016).
- [32] D. K. Schroder and D. L. Meier, *IEEE Trans. Electron Devices* **31**, 637 (1984).

- [33] S. Y. Lee, H. Choi, H. Li, K. Ji, S. Nam, J. Choi, S. W. Ahn, H. M. Lee, and B. Park, *Sol. Energy Mater. Sol. Cells* **120**, 412 (2014).
- [34] G. J. Bauhuis, P. Mulder, E. J. Haverkamp, J. C. C. M. Hujiben, and J. J. Schermer, *Sol. Energy Mater. Sol. Cells* **93**, 1488 (2009).
- [35] K. Kuribayashi, H. Matsumoto, H. Uda, Y. Komatsu, A. Nakano, and S. Ikegami, *Jpn. J. Appl. Phys.* **22**, 1828 (1983).
- [36] K. Nishioka, T. Takamoto, T. Agui, M. Kaneiwa, Y. Uraoka, and T. Fuyuki, *Sol. Energy Mater. Sol. Cells* **90**, 1308 (2006).
- [37] M. A. Khan, M. S. Shur, and Q. Chen, *Appl. Phys. Lett.* **68**, 3022 (1996).
- [38] L. L. Smith, R. F. Davis, M. J. Kim, R. W. Carpenter, and Y. Huang, *J. Mater. Res.* **12**, 2249 (1997).
- [39] R. Takabe, K. Nakamura, M. Baba, W. Du, M. Ajmal Khan, K. Toko, M. Sasase, K. O. Hara, N. Usami, and T. Suemasu, *Jpn. J. Appl. Phys.* **53**, 04ER04 (2014).
- [40] M. Kobayashi, Y. Matsumoto, Y. Ichikawa, D. Tsukada, and T. Suemasu, *Appl. Phys. Express* **1**, 051403 (2008).
- [41] Y. Inomata, T. Nakamura, T. Suemasu, and F. Hasegawa, *Jpn. J. Appl. Phys.* **43**, L478 (2004).
- [42] R. Takabe, H. Takeuchi, W. Du, K. Ito, K. Toko, S. Ueda, A. Kimura, and T. Suemasu, *J. Appl. Phys.* **119**, 165304 (2016).
- [43] P. N. Vinod, *J. Mater. Sci.: Mater. Electron.* **22**, 1248 (2011).
- [44] D. Tsukahara, M. Baba, K. Watanabe, T. Kimura, K. O. Hara, W. Du, N. Usami, K. Toko, T. Sekiguchi, and T. Sumasu, *Jpn. J. Appl. Phys.* **54**, 030306 (2015).
- [45] K. D. Hobart, D. J. Godbey, M. E. Twigg, M. Fatemi, and P. E. Thompson, *Surf. Sci.* **334**, 29 (1995).
- [46] A. Gulino, G. G. Condorelli, K. Fragala, and R. G. Egdell, *Appl. Surf. Sci.* **90**, 289 (1995).

Si

[47] R. Kaspi and K. R. Evans, *J. Cryst. Growth* **175**, 838 (1997).

[48] D. Reinking, M. Kammler, M. HornVonHoegen, and K. R. Hofmann, *Appl. Phys. Lett.* **71**, 924 (1997).

[49] O. J. Pitts, S. P. Watkins, C. X. Wang, V. Fink, and K. L. Kavanagh, *J. Cryst. Growth* **254**, 28 (2003).

[50] H. S. Wong, L. Chan, G. Sainudra, and Y. C. Yeo, *IEEE Trans. Electron Devices* **18**, 703 (2007).

[51] M. Oehme, J. Werner, and E. Kasper, *J. Cryst. Growth* **310**, 4531 (2008).

[52] D. V. Yurasov, A. V. Antonov, M. N. Drozdov, V. B. Schmagin, K. E. Spirin, and A. V. Novikov, *J. Appl. Phys.* **118**, 145701 (2015).

Figure captions

Fig. 1 θ - 2θ XRD and RHEED patterns observed along the Si $[1\bar{1}\bar{2}]$ azimuth of samples A, B, C, and D. The asterisk (*) indicates the diffraction of the Si substrate used.

Fig. 2 Sample structure for R_C measurement and the relationships between resistance and Al or ITO electrode distance for sample C, Sb-doped n-BaSi₂ ($n = 2.4 \times 10^{18} \text{ cm}^{-3}$).

Fig. 3 R_C as a function of electron concentration for Al/n-BaSi₂ and ITO/n-BaSi₂. The smallest R_C ($0.35 \Omega \text{ cm}^2$) obtained from Al/p-BaSi₂ [31] is shown for comparison.

Fig. 4 SIMS depth profile of Sb atoms and secondary ions (Ba + Si).

Fig. 5 Sample structure of sample F and RHEED patterns of each layer observed along the Si $[\bar{1}\bar{1}0]$ azimuth.

Fig. 6 θ - 2θ XRD pattern of sample F. The asterisk (*) indicates the diffraction of the Si substrate used.

Fig. 7 IQE spectrum of sample F under a bias voltage of -0.1 V applied to the surface ITO electrode with respect to the back side-surface Al electrode.

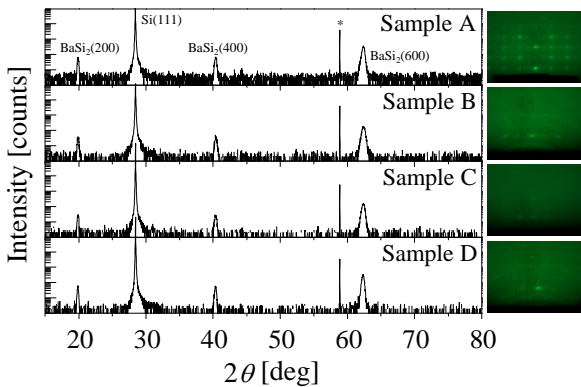


Fig. 1

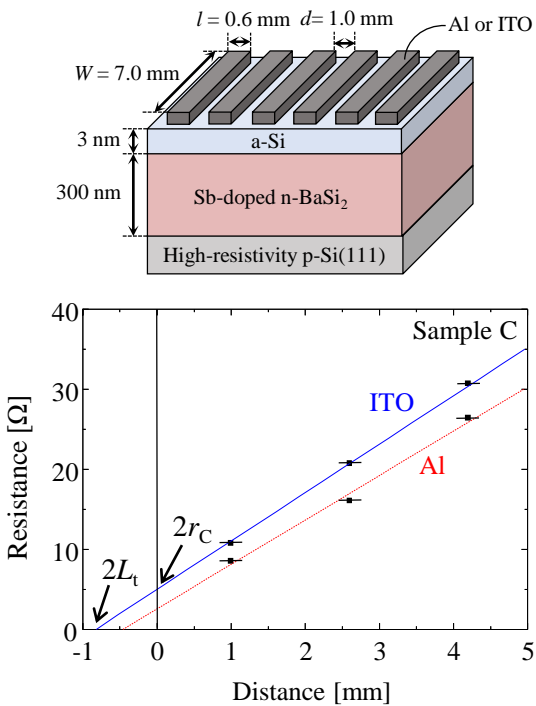


Fig. 2

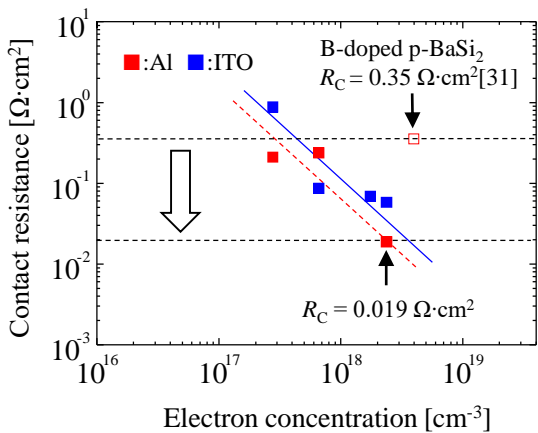


Fig. 3

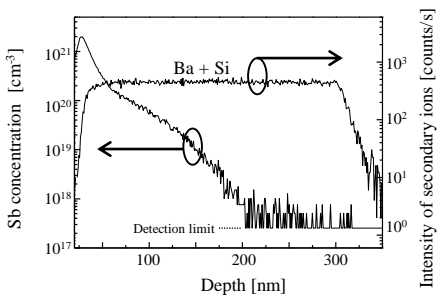


Fig. 4

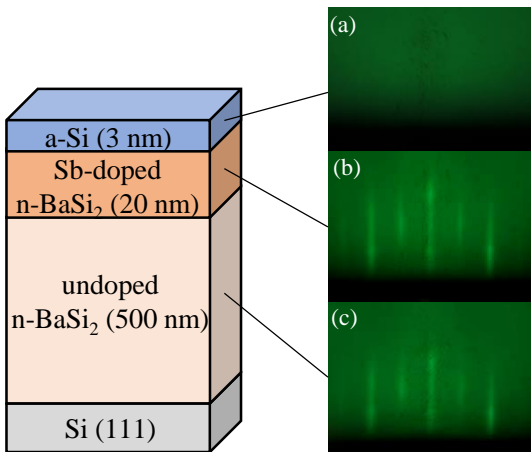


Fig. 5

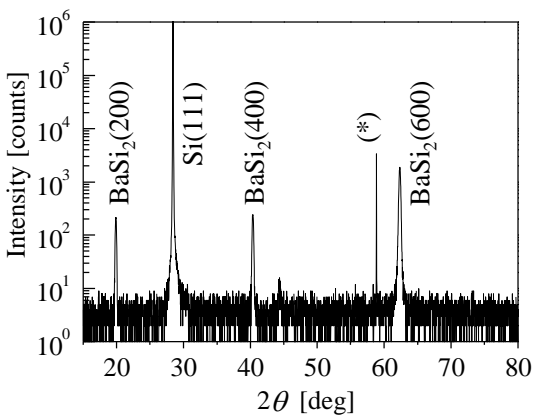


Fig. 6

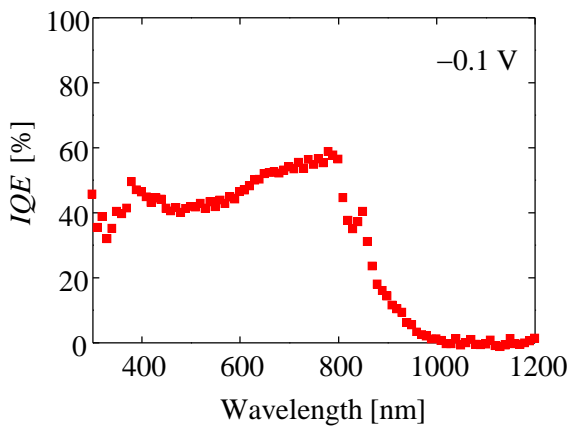


Fig. 7